Theoretical and Applied Fracture Mechanics 139 (2025) 105137

Contents lists available at ScienceDirect

Theoretical and Applied Fracture Mechanics

journal homepage: www.elsevier.com/locate/tafmec

Investigation of cracking resistance of rubberized epoxy asphalt mixture using semi-circular bending (SCB) test

Chenguang Shi [a], Tianling Wang [b,*], Peng Guo [a], Yulou Fan [c,d], You Wu [e], Jun Yang [c,*]

[a] National & Local Joint Engineering Research Center of Transportation and Civil Engineering Materials, Chongqing Jiaotong University, PR China
[b] Institute of Highway Engineering (ISAC), RWTH Aachen University, Mies-van-der-Rohe-Street 1, 52074 Aachen, Germany
[c] School of Transportation, Southeast University, #2 Southeast University Road, Nanjing 211189, PR China
[d] Department of Civil and Environmental Engineering, The Hong Kong Polytechnic University, Kowloon, Hong Kong
[e] Faculty of Civil Engineering and Geoscience, Delft University of Technology, Stevinweg 1, 2628 CN Delft, the Netherlands

ARTICLE INFO

Keywords:
Rubberized epoxy asphalt mixture
Crack resistance
P-value
Loading rate
Temperature
CR content

ABSTRACT

The dry-mixed rubberized epoxy asphalt mixture (DREAM) has demonstrated superior mechanical properties. The addition of crumb rubber (CR) improves the damping performance and toughness characteristics of DREAM while offering significant potential for recycling waste materials. However, cracking remains a critical issue for DREAM, necessitating further experimental investigations into its crack resistance performance, especially regarding the sensitivity of evaluation indicators. In this study, semi-circular bending tests were conducted on DREAM with varying CR content under three loading rates and two test temperatures. P-values were utilized to evaluate the sensitivity of nine indicators. Results suggest that not all fracture performance indicators exhibit significant differences due to the varying toughness resulting from the CR content in DREAM. Normalized parameters, such as the pre- and total cracking resistance index (CRI^{pre}, *CRI*), tensile stiffness index (*TSI*), and tensile strength (*TS*) demonstrate superior performance in distinguishing the effects of CR content and test temperature. Meanwhile, *TSI*, *CRI*, and CRI^{pre} can only significantly distinguish the effects of loading rate in DREAM with high CR content. Moreover, the addition of CR reduces the load-bearing capacity and stiffness of DREAM while increasing its flexibility and crack propagation resistance. Among the effective indicators, *TSI* is more sensitive to changes in loading rate and test temperature compared to CRI^{pre} and *CRI*. This study aims to enhance the understanding of the crack resistance performance and indicator adaptability of DREAM via macro-mechanical experiments and provides guidance for its future applications.

1. Introduction

Rubberized epoxy asphalt mixtures have gained attention due to their enhanced damping performance and toughness characteristics in track infrastructure [1–5]. Although these mixtures demonstrate favorable technical properties, their performance is limited by cracking issues stemming from insufficient adhesion between crumb rubber (CR) and bitumen [1,6,7]. This interfacial weakness, exacerbated by traffic loading and environmental factors, necessitates a thorough investigation on the cracking behavior of the mixture under various service conditions.

To assess the cracking resistance performance of materials, two primary methods are commonly employed: repeated loading beam fatigue tests and surrogate monotonic fracture tests [8,9]. The repeated loading approach determines the fatigue life of materials, albeit in a labor-intensive manner. This method quantifies fatigue life by measuring the number of load cycles required to reach a predefined level of damage. In contrast, the monotonic fracture test necessitates less complex and expensive testing apparatus, shorter experimental durations, and simpler specimen preparation protocols. Although the monotonic fracture test does not directly measure fatigue life, numerous studies have established a strong correlation between fracture resistance and fatigue performance by calculating parameters such as toughness or the critical strain energy release rate [10]. This technique has emerged as a promising analytical tool, facilitating a comparative evaluation of various asphalt materials in terms of their cracking resistance. Fracture

* Corresponding authors.
E-mail addresses: chenguangshi@cqjtu.edu.cn (C. Shi), t.wang@isac.rwth-aachen.de (T. Wang), guopeng@cqjtu.edu.cn (P. Guo), yulou_fan@126.com (Y. Fan), You.Wu@tudelft.nl (Y. Wu), yangjun@seu.edu.cn (J. Yang).

https://doi.org/10.1016/j.tafmec.2025.105137
Received 25 January 2025; Received in revised form 10 July 2025; Accepted 29 July 2025
Available online 30 July 2025

Table 1
Design gradations (%) of four DREAMs by V-S method.

Sieve size/mm	26.5	19.0	16.0	13.2	9.5	4.75	CR	1.18	0.6	0.3	0.15	0.075	filler
EA-6CR	13.4	9.6	8.9	9.7	12.9	3.5	6.0	7.2	5.2	3.9	2.9	2.1	5.7
EA-4CR						8.5	4.0						
EA-2CR						13.5	2.0						
EA-0CR						18.5	0.0						

testing can be performed on both beam and cylindrical specimens, utilizing methods such as semi-circular bending (SCB), indirect tensile, disk-shaped sharp tensile, and notched three-point bending tests [11–16]. Among these methodologies, the SCB is one of the most widely employed surrogate monotonic fracture tests for evaluating crack propagation in asphalt mixtures [11,17–21].

Various parameters can be derived from the load-line displacement (LLD) curve recorded during the SCB test to characterize the fracture resistance of asphalt mixtures [22–25]. Typically, the curve delineates two distinct phases: an initial phase characterized by an increasing force required for the onset of fracture (pre-peak), followed by a subsequent phase marked by a reduction in force as the crack propagates through the specimen (post-peak). By extracting one or several parameters from these two phases, such as peak load, area under the curve, and the slopes of both post- and pre-peak curves, performance indicators including fracture energy, flexibility index (*FI*), toughness index (*TI*), cracking resistance index (*CRI*), tensile stiffness index (*TSI*), and tensile strength (*TS*) can be determined.

Fracture energy, from the view of fracture mechanics, represents the energy required to create a unit surface area of fracture within the asphalt mixture, making it a widely used metric for evaluating the fracture resistance of asphalt mixtures. Typically, it is divided into pre-peak and post-peak components to evaluate crack initiation and propagation separately. However, relying solely on fracture energy is insufficient for ranking cracking resistance due to the viscoelasticity dependency of asphalt mixtures. Specifically, two different types of asphalt mixtures may exhibit identical total energy to failure; one may demonstrate a high peak-load value coupled with a low end-displacement value, while the other may present a low peak-load value alongside a high end-displacement value. Consequently, a novel performance-based index based on fracture mechanics, *FI*, has been proposed by combining the effects of fracture energy and the post-peak slope of the load–displacement curve [26]. The slope characterizes the brittleness of the mixture due to rapid unloading after crack initiation; therefore the *FI* tends to evaluate the ductility of the mixture rather than its stiffness [19]. Nonetheless, there is a weak correlation coefficient between the fracture energy and *FI*, which can be attributed to the significant variability in the slope. Additionally, *TI* is defined as the product of post-peak fracture energy and the displacement between the maximum load and 50 % of the maximum post-peak load, serving to assess the brittle behavior of asphalt mixtures [27]. In comparison to *FI*, *TI* exhibits a lower coefficient of variation. Nevertheless, *TI* is similar to *FI*, which is heavily influenced by post-peak fracture evolution. This makes *TI* potentially unsuitable for brittle mixtures such as the epoxy asphalt mixture studied in this study. The reason is that the brittle mixtures tend to fracture completely upon reaching the peak load, making it challenging to extract relevant parameters associated with the post-peak phase. In this regard, Kaseer proposed *CRI* by normalizing the total fracture energy [28]. The *CRI* serves as a measure that quantifies the mechanical behavior of an asphalt mixture by comparing the energy required to fracture a sample with the strength of the mixture.

Based on this concept, a new crack resistance parameter, CRI^{pre}, is proposed in this study, which normalizes the pre-peak fracture energy to evaluate the crack resistance during the initiation process. A larger CRI^{pre} and *CRI* value suggest a more flexible asphalt mixture in both crack initiation and the overall process. Whereas a lower *CRI* value points to a brittle mixture. Additionally, crack propagation is influenced by the strength and stiffness of the asphalt mixture. An ideal asphalt mixture should exhibit both stiffness and flexibility [29,30]. Two indices, *TSI* and *TS*, have been proposed to investigate the cracking resistance performance of asphalt mixtures [27,31].

Although these proposed parameters each possess distinct merits, their applicability varies across different types of rubberized epoxy asphalt mixtures under diverse test conditions. Rubberized epoxy asphalt mixtures, characterized as viscoelastoplastic materials, exhibit different cracking evolution and resistance performance influenced by temperature, loading rate, and CR content [6,21,30,32,33]. Within the current framework of experimental procedures, the determination of testing temperature and loading rate is typically guided by practical experience and considerations of operational simplicity. Al-Qadi et al. analyzed the fracture resistance performance of asphalt mixtures using SCB tests across a spectrum of temperatures ranging from −30 °C to 30 °C, concurrently varying the loading rates from 5 to 100 mm/min [26]. Based on the obtained fracture energy values, they suggested that the SCB fracture test should be conducted at a moderate temperature of 25 °C and a rapid loading rate of 50 mm/min, as these conditions yielded the most favorable fracture energy results in their research. However, this recommendation lacks sufficient evidence and theoretical support. Zhou et al. deem that the selected loading rate may be excessively rapid to obtain enough data points for calculating the aforementioned indicators in the case of brittle materials, such as the epoxy asphalt mixture [34]. Simultaneously, excessively low loading rates are also problematic due to the introduction of creep damage [33].

This study aims to first evaluate the fracture resistance and toughening effect of the epoxy asphalt mixture containing varying CR content. The characterization parameters include total, pre- and post-peak fracture energy, *TI*, *CRI*, CRI^{pre}, *TSI*, and *TS*. Subsequently, SCB tests were conducted on rubberized epoxy asphalt mixtures with varying CR contents to elucidate the sensitivity of the fracture indicators. Test conditions were standardized, maintaining a fixed temperature of 25 °C across multiple loading rates, with a loading rate of 1 mm/min under two temperature conditions. The P-value analysis was performed on the results to identify statistically significant differences among the various types of asphalt mixtures and test conditions. Moreover, the effects of loading rate and temperature were evaluated to guide the selection of appropriate testing conditions that more accurately characterize the contribution of CR.

2. Experimental and parametric analysis methods

2.1. Mix design and specimen preparation

In this study, the dry-mixed rubberized epoxy asphalt mixtures (DREAM) with a nominal maximum aggregate size of 26.5 mm were prepared. The composition of DREAM was designed according to the V-S method, which is a volumetric mix design based on a multi–supported skeleton for asphalt mixtures [35,36]. In this design, aggregates of 4.75 mm occupy the largest proportion. Therefore, this type of coarse aggregate was replaced by CR of the same particle size in varying proportions to enhance resilience and energy dissipation within the asphalt mixture. Four types of DREAMs were formed: EA-0CR, EA-2CR, EA-4CR, and EA-6CR (the numbers represent the mass ratio of CR to the total aggregates). The gradation design of these four types of DREAMs with varying CR contents is shown in Table 1. The comprehensive

Table 2
Technical indicators of SBS modified asphalt.

Technical Indicators	Requirement	Result
Penetration (25 °C, 100 g, 5s) /0.1 mm	40 ~ 60	56
Ductility (5 °C, 5cm/min) /mm	≥20	31
Softening point /°C	≥60	88
Flash point /°C	≥230	> 300
Recovery of elasticity /%	≥75	94
Viscosity (135 °C) /Pa·s	≤3	2.245

Table 3
Technical indicators of resin and curing agent.

Material type	Technical Indicators	Requirement	Result
Resin	Viscosity (135 °C) /mPa·s	1000 ~ 5000	3110
	Flash point /°C	≥220	234
	Specific gravity (23 °C)	1.0 ~ 1.2	1.132
Curing agent	Viscosity (135 °C) /mPa·s	100 ~ 800	186
	Flash point /°C	≥145	163
	Specific gravity (23 °C)	0.8 ~ 1.0	0.906

understanding of the detailed design process of DREAM and the material property parameters used in the asphalt mixture are referred to previous research [6]. Mineral aggregates and filler consisted exclusively of limestone. To enhance the fracture resistance of the epoxy asphalt binder, the modified asphalt binder containing 4 % Styrene-Butadiene-Styrene (SBS) polymers was utilized. The technical specifications of the materials are presented in Table 2. The epoxy system, comprising resin and curing agent at a mass ratio of 56:44, was blended with the modified asphalt binder at a 1:1 mass ratio. Their technical specifications are presented in Table 3. Density measurements of the epoxy asphalt binder conducted by JTG E20-2011 (China 2011) yielded a value of 1.05 g·cm^{-3}. The CR incorporated into the DREAMs via a dry process was processed from waste tires, with a density of 1.02 g·cm^{-3} and a nominal size of 4.75 mm.

The cylindrical specimens for the SCB test were prepared using gyratory compaction, resulting in a diameter of 150 mm and a height of 170 mm. Each specimen was subsequently cut into six semicircles with a height of 45 mm. A standardized notch of 15 mm in length and 2 mm in width was precisely machined at the midpoint of the straight edge along the thickness direction (as shown in Fig. 1) [37–39]. To ensure experimental consistency, three semicircles extracted from a single cylindrical specimen were tested under each condition.

2.2. Experimental program

The SCB tests were conducted using a universal testing machine (UTM), as illustrated in Fig. 2. The system is equipped with a load cell that has a maximum load capacity of 100 kN and a measurement accuracy of 0.01 N. Prior to testing, the specimens were placed in an environmental chamber at the testing temperature for 3 h to ensure a consistent internal temperature. The supports beneath the specimen were symmetrically positioned with a span of 120 mm. To clarify the effects of CR content, temperature, and loading rate on the fracture resistance of DREAM, four types of mixtures were tested under three loading rates and two test temperatures. Considering the creep behavior and brittleness of DREAM, the minimum and maximum loading rates were set at 1 and 10 mm/min. And the test temperatures were set at 15 and 25 °C. In each test condition, three replicate SCB samples were tested. Table 4 presents the specifications of the test specimens and detailed testing conditions. Due to the brittle rupture of EA-0CR at 25 °C with a loading rate of 10 mm/min, there were insufficient data points to calculate the indicators; therefore, this loading rate was excluded from the analysis.

2.3. Fracture indicators

The crack behavior of DREAM is evaluated using various fracture indicators obtained from the load–displacement curve in the SCB test, including fracture energy, *FI*, *TI*, *CRI*, *TSI*, and *TS*.

After the specimens were fractured, the fracture energy (G_f) is determined by calculating the ratio of fracture work to the ligament area as shown in Eqs. (1) and (2). As discussed in the Introduction, G_f is divided into G_f^{pre} and G_f^{post} based on the peak load in the

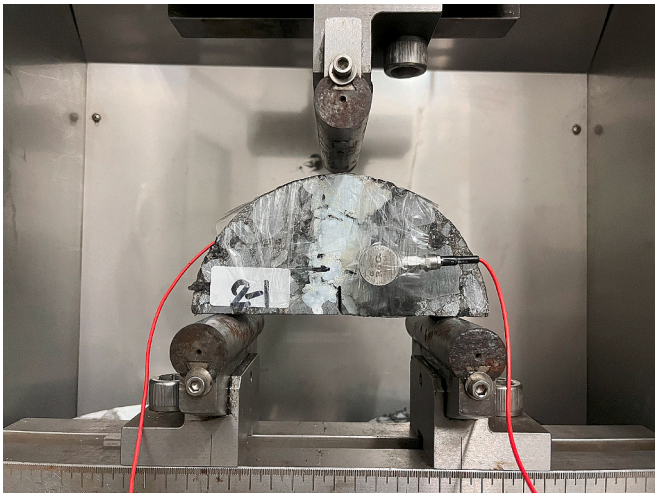

Fig. 2. SCB test setup and specimen.

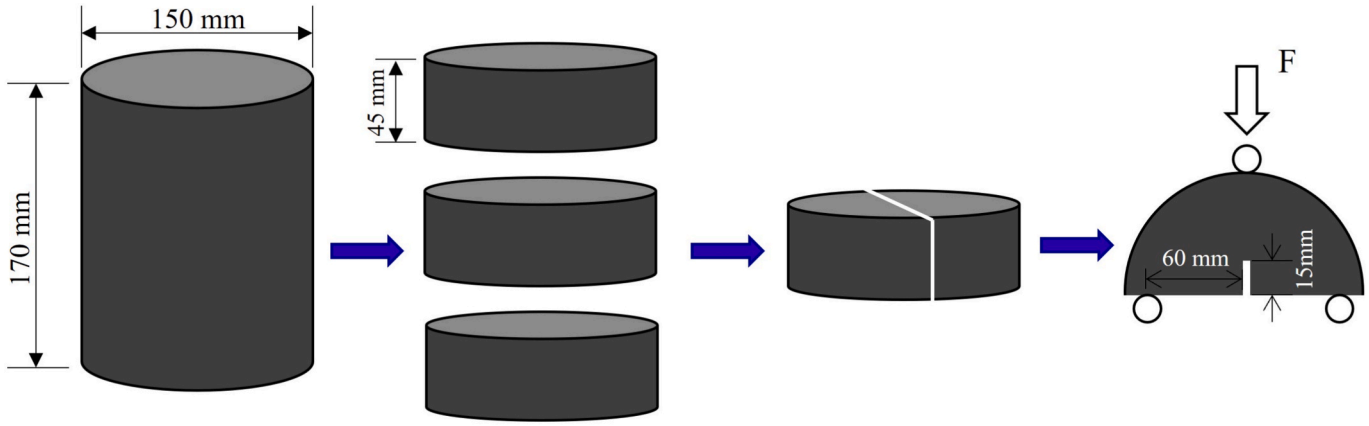

Fig. 1. Schematic illustration of specimen preparation and loading configuration.

Table 4
Specifications of fracture test conducted on the SCB specimens made of different DREAM.

Type	Temperature (°C)	Loading rate (mm/min)	Temperature (°C)	Loading rate (mm/min)
EA-6CR	25	1, 5, 10	15	1
EA-4CR		1, 5, 10		
EA-2CR		1, 5, 10		
EA-0CR		1, 5		

load–displacement curve, as shown in Eq. (3). The G_f^{pre} represents the initiation of cracking, while G_f^{post} is selected based on the mechanism of fracture process zone formation in quasi-brittle mixtures [40].

The indicators *FI*, *TI*, as well as *CRI*, which are utilized to better understand the crack propagation in DREAM, are calculated based on Eqs. (4) to (6). According to the definition and calculation of *CRI*, the CRI^{pre} parameter, which normalizes the pre-peak fracture energy, is proposed in this study to evaluate crack resistance during the initiation process. It can be calculated based on Eq. (7).

Additionally, *TSI* and *TS*, shown in Eqs. (8) and (9), are two indicators to evaluate the stiffness and strength of DREAM, which also influence the crack propagation rate.

$$G_f = \frac{W_f}{A_{lig}} \tag{1}$$

$$A_{lig} = (R - a) \times t \tag{2}$$

$$G_f = G_f^{pre} + G_f^{post} \tag{3}$$

where, G_f is the fracture energy in J/m^2; W_f is the work of fracture in J; A_{lig} is the ligament area in m^2; R is the radius of specimen; t is the specimen thickness; a is the notch length.

$$FI = 0.01 \times \frac{G_f}{|m|} \tag{4}$$

$$TI = G_f^{post} \times \left(D_{tough} - D_{strength}\right) \times 0.001 \tag{5}$$

$$CRI = \frac{G_f}{P_{\max}} \tag{6}$$

$$CRI^{pre} = \frac{G_f^{pre}}{P_{\max}} \tag{7}$$

$$TSI = \frac{0.5P_{\max}}{D_{stiffness}} \tag{8}$$

$$TS = \frac{P_{\max}}{A_{lig}} \tag{9}$$

where, m is the slope at the post-peak inflection point; $D_{stiffness}$, $D_{strength}$, and D_{tough} are the displacement at 50 % pre P_{max}, P_{max} and 50 % post P_{max}, respectively; P_{max} is the peak load.

2.4. Indicator adaptability analysis

To evaluate the adaptability of different fracture indicators, 16 groups of DREAM specimens were subjected to SCB tests. Three factors including CR content, loading rate, and test temperature were considered. Statistical significance corresponding to the nine types of fracture indicators across the 16 groups of DREAM specimens was determined through P-value analysis. And their sensitivity under varying test conditions was identified by P-values below 0.05, which indicate significant effects at a 95 % confidence interval. For assessing fracture indicators sensitivity to CR content, four groups were tested at 25 °C with loading rates of 1, 5, and 10 mm/min, and at 15 °C with a loading rate of 1 mm/min. To evaluate sensitivity to loading rate, four groups were analyzed at 25 °C with CR contents of 0 %, 2 %, 4 %, and 6 %. For sensitivity to test temperature, four groups were examined at a loading rate of 1 mm/min with CR contents of 0 %, 2 %, 4 %, and 6 %.

Tukey's Honestly Significant Difference (HSD) test was performed on fracture indicators that showed significant sensitivity ($P < 0.05$) to CR content, loading rate, and temperature. The analysis was conducted to identify statistically significant pairwise differences. A 95 % confidence level ($\alpha = 0.05$) was used, and groupings were reported using letter labels (e.g., A, B, C).

3. Results and discussion

3.1. Sensitivity analysis of fracture indicators

3.1.1. Sensitivity to CR content

The corresponding P-values of fracture indicators related to the CR content are presented in Table 5. It can be observed that the P-values for all fracture indicators exceed 0.05 when the loading rate reaches 10 mm/min, with the exception of G_f^{post} and CRI^{pre}. This indicates that the fracture indicators no longer demonstrate significant differences at this loading rate. It may be attributed to two aspects: First, the excessive loading rate results in an insufficient number of load–displacement data points, leading to inaccurate calculations of the fracture indicators. For instance, it was not possible to collect sufficient data points for EA-0CR at a test temperature of 25 °C and a loading rate of 10 mm/min. Second, the higher loading rate induces more pronounced brittle fracture in DREAM, increasing the variability among replicates. This variability may diminish the effect of CR content. Therefore, it can be concluded that a loading rate of 10 mm/min is not suitable for evaluating the influence of CR content on fracture performance, as the fracture indicators fail to effectively differentiate the crack resistance performance.

The statistical significance of fracture energy indicators (G_f, G_f^{pre}, G_f^{post}) regarding different DREAMs also varies with loading rates and temperature conditions. For example, G_f and G_f^{post} can significantly distinguish various DREAMs only at a test temperature of 15 °C and a loading rate of 1 mm/min, whereas G_f^{pre} achieves this distinction solely at 25 °C and a loading rate of 1 mm/min. The fracture energy parameters of DREAMs with varying CR content at 25 °C and a loading rate of 1

Table 5
Statistical P-value of fracture indicators for different DREAMs at two test temperatures and three loading rates.

Loading rate (mm/min)	Temperature (°C)	CR content (wt%)	G_f	G_f^{pre}	G_f^{post}	*FI*	*TI*	*CRI*	*TSI*	*TS*	CRI^{pre}
1	25	0/2/4/6	0.054	0.009	0.104	0.068	0.123	0.001	0.000	0.000	0.000
5		0/2/4/6	0.272	0.066	0.431	0.000	0.101	0.012	0.003	0.005	0.143
10		2/4/6	0.076	0.347	0.018	0.350	0.196	0.190	0.089	0.283	0.044
1	15	0/2/4/6	0.026	0.375	0.000	0.261	0.000	0.000	0.000	0.000	0.013

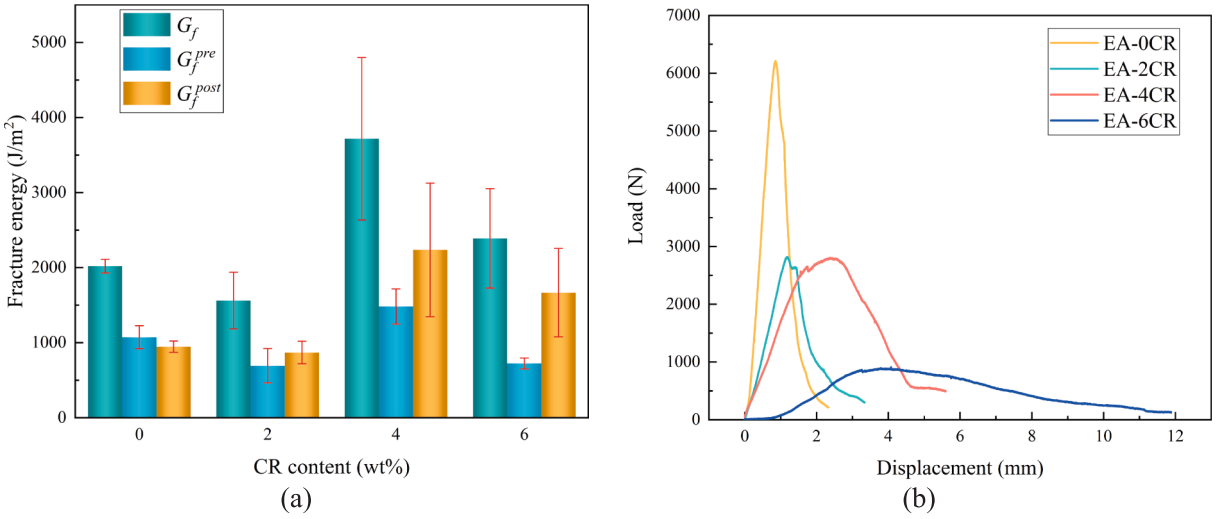

Fig. 3. Fracture results of DREAM under 25 °C and a loading rate of 1 mm/min: (a) Fracture energy; (b) Load-displacement curve.

mm/min are presented in Fig. 3(a). The results under other loading conditions are similar and therefore not elaborated here. It is evident that the fracture energy parameters do not change monotonically with CR content; instead, they exhibit a peak at 4 wt%. Moreover, the values of EA-6CR are higher than those of EA-0CR and EA-4CR. Under identical testing conditions, the epoxy asphalt mixtures in this study demonstrate significantly higher fracture energy compared to conventional base asphalt mixtures, irrespective of the rubber particle content. For comparison, Chen et al. [33] reported a fracture energy of approximately 0.65 kJ/m^2 for mixtures with PG58-28 binder, while other studies documented values of 0.38 kJ/m^2 and 0.14 kJ/m^2 for mixtures containing PG 64–22 and PG 52–28 binders, respectively [37]. Further analysis of the load–displacement curves of DREAMs (shown in Fig. 3 (b)) reveals that the addition of CR significantly increases the toughness of DREAMs. The load–displacement curve becomes smoother and more extended, which is reflected by a reduction in peak load and an increase in $D_{strength}$ and D_{tough}. However, these two changes exert opposite effects on G_f. The former reduces the fracture energy, while the latter increases it. With respect to EA-4CR, the reduction in peak load is comparable to that of EA-2CR; whereas, the $D_{strength}$ and D_{tough} are significantly larger, resulting in a peak in fracture energy of EA-4CR. Consequently, the fracture energy indicators are considered inadequate for clearly distinguishing the effect of CR content on DREAMs under varying loading rates and test temperatures.

Table 5 indicates that the exhibition of *FI* and *TI* is relatively insensitive to the overall performance of different DREAMs. This insensitivity of the *FI* indicator may stem from its calculation, which involves both the fracture energy and the absolute value of the post-peak slope. As shown in Fig. 3(b), the change in G_f does not synchronize with the change in the post-peak slope as CR content increases, potentially resulting in negligible fluctuations in the *FI* indicator. The large P-value for the *TI* indicator is primarily attributed to the increase in both G_f^{post} and fracture displacement at CR contents of 4 wt% or 6 wt%. The influences of CR content on the fracture performance of DREAMs become more pronounced when using the product of G_f^{post} and fracture displacement, making the *TI* indicator less significant.

In contrast, the *CRI*, CRI^{pre}, *TSI*, and *TS* indicators, which are normalized with respect to G_f or P_{max}, show satisfactory sensitivity to different DREAMs under varying test temperatures and loading rates. Therefore, these four fracture indicators are considered statistically significant for evaluating the influence of CR content on the fracture performance of DREAMs.

3.1.2. Sensitivity to loading rate and temperature

The fracture indicators of DREAM with varying CR content under three loading rates at 25 °C are analyzed for evaluating their sensitivity to loading rates. The corresponding P-values are presented in Table 6. It is observed that the loading rate generally does not exhibit a significant difference in fracture energy parameters, with only a few exceptions, such as G_f^{pre} of EA-2CR and G_f^{post} of EA-0CR. For the *FI* and *TI* parameters, no significant differences are identified. Furthermore, *TS* can only distinguish the significance of one DREAM group under different loading rates, which occurs at lower CR content. In addition, *TSI*, CRI^{pre}, and *CRI* exhibit similar trends, where the effects of loading rates can be significantly distinguished for DREAM with higher CR content. These three indicators may be suitable for DREAMs with stronger toughness.

Similar to the fracture indicator results of DREAM with varying CR content, the brittleness of DREAM increases the variability of fracture energy indicators among replicates across these three loading rates. This leads to closely aligned group means and reduced inter-group variation compared to intra-group one. For *FI* and *TI*, their calculations involve both fracture energy and the absolute value of the post-peak slope. While *TS* only considers P_{max}, which limits these indicators from displaying significant differences. Therefore, the *TSI, CRI*, and CRI^{pre} indicators are used in the subsequent analysis of the effect of loading rate on DREAM.

The P-values of fracture indicators at two test temperatures are calculated and presented in Table 7, with the loading rate set at 1 mm/min. Results indicate that no fracture energy parameter generally exhibits significant differences in response to test temperature across all

Table 6
Statistical P-value of fracture indicators for different DREAMs at three loading rates.

CR content (wt%)	Temperature (°C)	Loading rate (mm/min)	G_f	G_f^{pre}	G_f^{post}	*FI*	*TI*	*CRI*	*TSI*	*TS*	CRI^{pre}
0	25	1/5	0.819	0.425	0.009	0.468	0.063	0.098	0.475	0.335	0.777
2		1/5/10	0.097	0.035	0.164	0.536	0.588	0.591	0.400	0.000	0.389
4		1/5/10	0.187	0.335	0.220	0.263	0.234	0.021	0.022	0.144	0.001
6		1/5/10	0.663	0.365	0.528	0.140	0.092	0.004	0.050	0.163	0.001

Table 7
Statistical P-value of fracture indicators for different DREAMs at two temperatures.

CR content (wt%)	Loading rate (mm/min)	Temperature (°C)	G_f	G_f^{pre}	G_f^{post}	*FI*	*TI*	*CRI*	*TSI*	*TS*	CRI^{pre}
0	1	15/25	0.621	0.027	0.003	0.253	0.006	0.001	0.007	0.010	0.075
2		15/25	0.038	0.011	0.765	0.193	0.158	0.082	0.080	0.005	0.386
4		15/25	0.094	0.364	0.079	0.072	0.114	0.007	0.027	0.004	0.001
6		15/25	0.286	0.115	0.904	0.756	0.070	0.002	0.005	0.000	0.001

Table 8
Tukey's comparison for different DREAMs at two temperatures and two loading rates.

Fracture indicator	*CRI*			*TSI*			*TS*			CRI^{pre}		
Loading condition	1	2	3	1	2	3	1	2	3	1	2	3
EA-0CR	A	A	A	A	A	A	A	A	A	A	A	A
EA-2CR	A	AB	B	B	AB	B	B	A	B	A	A	A
EA-4CR	AB	AB	B	BC	B	B	B	AB	BC	B	A	AB
EA-6CR	C	B	C	C	B	B	C	B	C	C	A	B

Note: 1, 2, and 3 represent the loading conditions of 1 mm/min at 25 °C, 5 mm/min at 25 °C, and 1 mm/min at 15 °C.

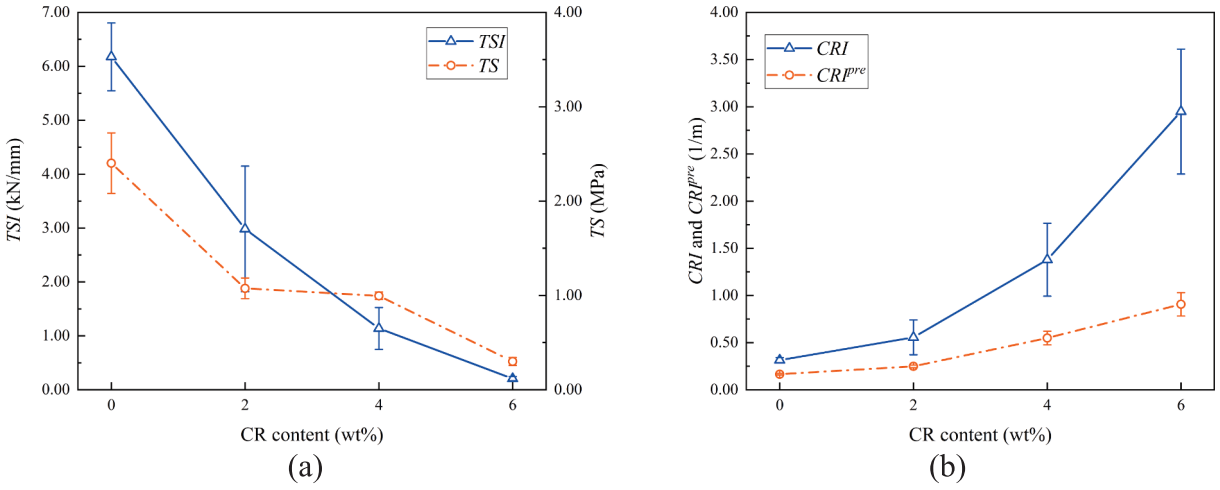

Fig. 4. Fracture indicators of DREAM with varying CR content: (a) TS and TSI; (b) CRI and CRI^{pre}. Note: Test temperature at 25 °C and loading rate of 1 mm/min.

CR contents. Furthermore, *FI* and *TI* parameters fail to demonstrate significant differences among test temperatures, which is consistent with the conclusions drawn from the significance analysis of loading rates. However, the *TSI*, *TS*, and *CRI* parameters can distinguish the differences significantly under these two test temperatures except for EA-2CR. Therefore, in the subsequent analysis of the effect of test temperature on DREAM, the *TS*, *TSI*, and *CRI* parameters are employed.

3.1.3. Post-hoc analysis of group differences in sensitive indicators

Tukey's HSD results (Table 8) show an examination of group-wise statistical differences across varying CR contents under different loading conditions. The grouping letters (A, B, and C) reflect statistically distinct subsets, with non-overlapping letters indicating significant differences between groups. It is revealed that among the four CR content levels, the EA-6CR group demonstrates the most significant statistical separation across all fracture indicators and loading conditions. It is assigned to the most distinct group (Group C). This trend is particularly evident under a moderate temperature of 25 °C and a lower loading rate of 1 mm/min, where the fracture resistance is not affected by the increased brittleness. In contrast, groups overlapping for EA-2CR and EA-4CR suggest that intermediate CR contents result in gradual or transitional changes in identifying the indicators sensitivity. While these groups rarely differ significantly from each other, reflecting a limited ability to distinguish mechanical performance at moderate CR levels.

3.2. Effect of CR content

The trends of the fracture indicators *TS*, *TSI*, *CRI*, and CRI^{pre} of DREAM with varying CR contents under a loading rate of 1 mm/min and a test temperature of 25 °C are illustrated in Fig. 4. The results under other loading conditions are similar and will not be elaborated. *TSI* and *TS* (calculated using Eqs. (8) and (9) are employed to evaluate the strength and stiffness of DREAM. As shown in Fig. 4(a), EA-0CR (i.e., the epoxy asphalt mixture) demonstrates significantly higher crack strength (P_{max}) and stiffness compared to traditional asphalt mixtures, indicating that the epoxy asphalt mixture possesses superior resistance to maximum loads. However, both *TS* and *TSI* of DREAM show a negative correlation with CR content. With respect to EA-2CR, its *TS* decreases by more than 50 %, with a slight decline observed when the CR content is further increased to 4 wt%. As the CR content increases, the *TSI* value decreases at a nearly constant rate, with reductions of more than 50 % and 80 % in EA-2CR and EA-4CR, respectively. Materials with ideal fracture resistance are expected to undergo greater deformation before reaching the peak load. The crumb rubber particles significantly reduce the resistance to maximum loads, indicating that the addition of CR decreases the peak load-bearing capacity and stiffness of DREAM.

The CRI^{pre} values, which characterize the crack resistance of DREAM during crack initiation, and the *CRI* values, which correspond to the entire process of crack initiation and propagation, both show a monotonous increase with rising CR content. Simultaneously, the increase in

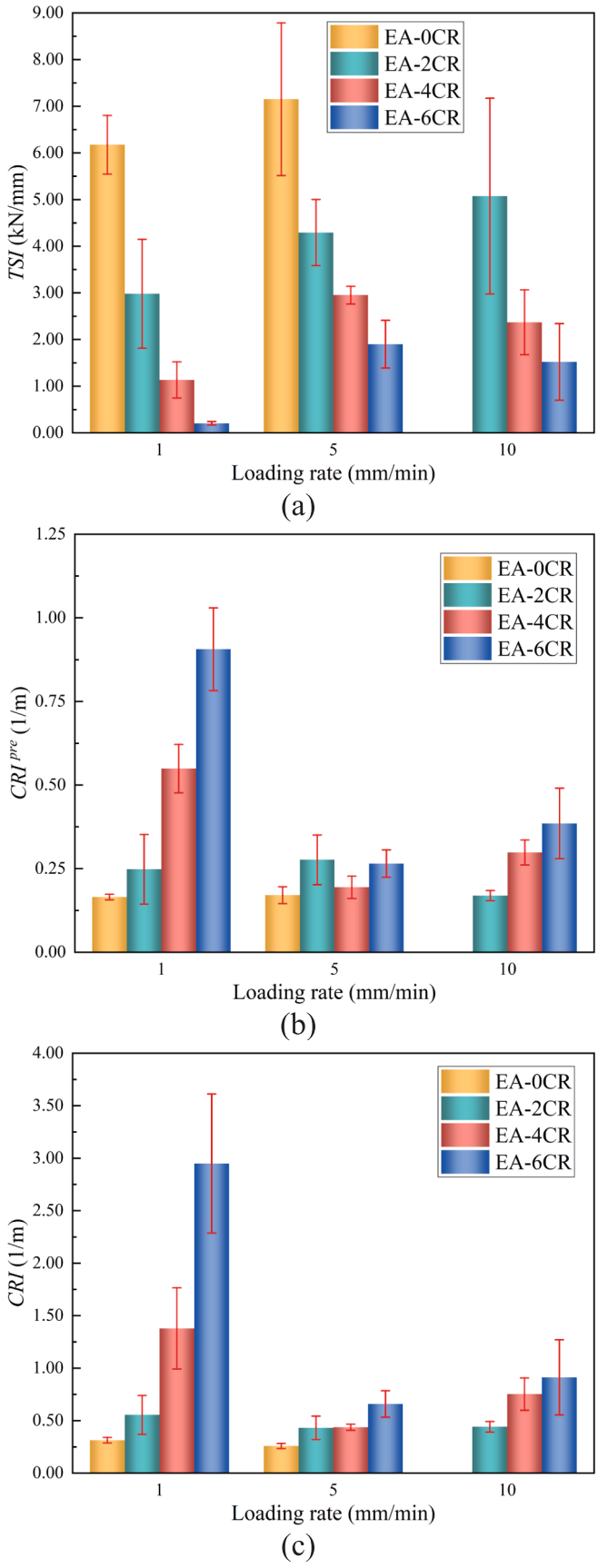

Fig. 5. Fracture indicators of DREAM at 25 °C and three loading rates: (a) TSI; (b) CRI^{pre}; (c) CRI.

CRI values is significantly greater than that of CRI^{pre}. It can also be observed in Fig. 3(b) that the load–displacement curve transitions from a steep post-peak drop to progressively larger post-peak displacements. This indicates that the addition of CR particles enhances the flexibility and crack propagation resistance of DREAM after the crack formation. Consequently, the DREAMs become less brittle, thereby improving their performance in resisting crack propagation.

The observed changes in fracture indicators can be attributed to the reduced adhesion between the CR and the epoxy bitumen binder, which facilitates crack formation under load, as evidenced by the decrease in *TSI* and *TS* indicators. However, the presence of CR mitigates the stress concentration at the crack tip, thereby decelerating the rate of crack propagation. This phenomenon is reflected by the increase in CRI^{pre} and *CRI* values. Consequently, CR exhibits opposing effects on the resistance to crack initiation and propagation in DREAM. It is recommended to conduct a balance evaluation when implementing DREAM in applications, as a higher CR content in the DREAM is preferred to improve crack propagation resistance, provided that the requirements for fracture strength are satisfied.

3.3. *Effect of loading rate*

Based on the evaluation in Section 3.1.2, it can be concluded that no fracture indicators significantly distinguish the influence of loading rate on DREAM across all CR content. However, *TSI*, CRI^{pre}, as well as *CRI* can function effectively under high CR content. Therefore, these three indicators are selected to assess the influence of loading rates (1, 5, and 10 mm/min) on the fracture performance of DREAM. The fracture indicators at 25 °C are illustrated in Fig. 5.

It can be observed in Fig. 5(a) that the *TSI* of DREAM decreases with increasing CR content across all loading rates. However, DREAM mixtures with specific CR contents exhibit different trends under different loading rates. For DREAM with lower CR contents (0 wt% and 2 wt%), *TSI* shows a monotonic increase as the loading rate rises, indicating that low CR content has a limited effect on enhancing the toughness of DREAM. Conversely, for DREAM with higher CR contents (4 wt% and 6 wt%), *TSI* reaches a peak at 5 mm/min and then decreases as the loading rate rises to 10 mm/min. Taking EA-4CR as an example, the load–displacement curves at 25 °C across the three loading rates are shown in Fig. 6. The load–displacement curves for other DREAM mixtures show similar characteristics and are not discussed in detail here. Notably, increasing the loading rate from 1 to 5 mm/min influences the fracture behavior of DREAM similarly to reducing the CR content from 4 wt% to 0 wt%, resulting in steeper and shorter load–displacement curves. However, when the loading rate is further increased from 5 to 10 mm/min, the load–displacement curve resembles 1 mm/min. This suggests that CR improves the toughness of DREAM at higher loading rates, while simultaneously reducing its capacity to withstand peak loads.

As shown in Fig. 5 (b) and (c), all DREAMs present the same trend at loading rates of 1 and 10 mm/min, with the exception of 5 mm/min. Specifically, both CRI^{pre} and *CRI* generally exhibit a decreasing trend with increasing loading rates. Similar to *TSI*, the CRI^{pre} and *CRI* values of EA-6CR are higher than those of EA-4CR. This suggests that DREAMs with a higher CR content demonstrate greater overall resistance during the crack initiation and propagation processes under high loading rates.

To analyze the sensitivity of DREAM to loading rate, the relative changes in the three parameters of each DREAM are listed in Table 9. It is observed that the *TSI*, CRI^{pre}, and *CRI* parameters exhibit increased sensitivity to the loading rate as the CR content rises. For the virgin epoxy asphalt mixture, the relative changes in all three parameters from 1 to 5 mm/min remain within 20 %. Whereas these changes exceed 70 % when the CR content increases to 6 wt%. Furthermore, it is evident that *TSI* is more sensitive to loading rate compared to CRI^{pre} and *CRI*. Additionally, the enhancement in the toughness of DREAM due to high CR content is also reflected in the relative change observed at high loading rates: for all three parameters, the relative change when the

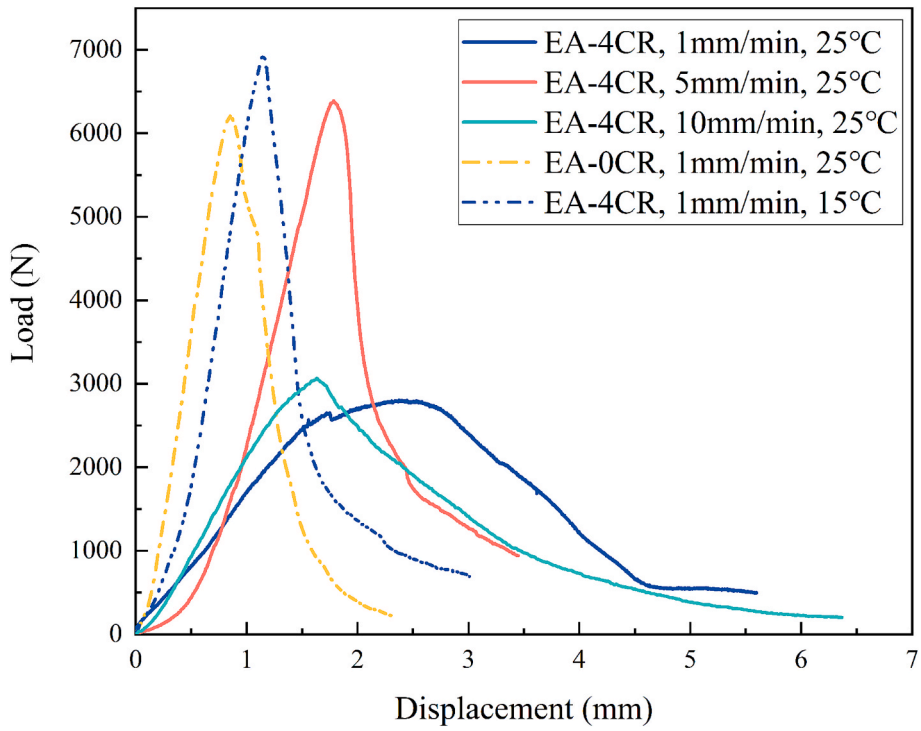

Fig. 6. Comparison of load–displacement curves of EA-0CR and EA-4CR under three loading rates and two test temperatures.

Table 9
Relative changes in three parameters of each DREAM when increasing the loading rate.

Relative change (%)	*TSI*		*CRI*^{pre}		*CRI*	
Loading rate (mm/min)	1 to 5	1 to 10	1 to 5	1 to 10	1 to 5	1 to 10
EA-0CR	15.8	–	3.4	–	−17.4	–
EA-2CR	43.9	70.1	11.3	−31.6	−22.2	−20.3
EA-4CR	159.6	108.5	−64.6	−45.6	−68.2	−45.4
EA-6CR	821.3	636.9	−70.8	−57.5	−77.7	−69.1

loading rate increases from 1 to 10 mm/min is less pronounced than that observed from 1 to 5 mm/min.

3.4. Effect of temperature

To analyze the effect of test temperature on the fracture performance of DREAM, the fracture indicators at a loading rate of 1 mm/min and test temperatures of 15 and 25 °C are illustrated in Fig. 7. The fracture performance indicators *TS*, *TSI*, and *CRI* are employed to evaluate the influence of test temperatures. It can be observed that these three indicators at 15°C exhibit trends similar to those at 25 °C. Namely, reducing the test temperature to 15 °C leads to an increase in both *TS* and *TSI* in terms of each DREAM, whereas *CRI* decreases. The load–displacement curves of EA-4CR at the two test temperatures are also presented as an example in Fig. 6. It can be observed that decreasing the test temperature has a comparable effect on the fracture process of DREAM to that of increasing the loading rate or reducing the CR content, as indicated by the steeper and shorter load–displacement curves. This suggests that lower test temperatures and higher loading rates produce similar effects: a stiffer and more rigid DREAM shows greater capacity to withstand peak loads and increased stiffness; however, its overall crack resistance during the initiation and propagation phases is reduced.

The temperature sensitivity of DREAM when decreasing from 25 to 15 °C is evaluated by calculating the relative changes in the three parameters of each DREAM, as listed in Table 10. Similar to the results of increasing the loading rate, the *TS*, *TSI*, and *CRI* parameters become more sensitive to test temperature as the CR content increases except for the *TS* value of EA-4CR. Additionally, *TS* and *TSI* are more sensitive to test temperature compared to *CRI*. In terms of virgin epoxy asphalt mixture, the relative changes in all three parameters remain below 80 %, whereas they can exceed tenfold when the CR content is increased to 6 wt%. It is also evident that the influence of temperature on fracture performance is significantly greater than that of the loading rate.

4. Conclusion and outlook

In this study, nine fracture indicators of epoxy asphalt mixtures containing CR obtained from SCB tests were evaluated to analyze their fracture resistance and toughness. These indicators include total, pre- and post-peak fracture energy, *TI*, *CRI*, *CRI*^{pre}, *TSI*, and *TS*. The P-value analysis was performed to elucidate the sensitivity of these fracture indicators among various types of asphalt mixtures and test conditions. SCB tests were conducted at the fixed temperature of 25 °C across multiple loading rates, at the same loading rates of 1 mm/min across two temperature conditions, and under the same testing conditions with varying CR content. Moreover, the effects of loading rate and temperature on the fracture performance of DREAM were evaluated. Several conclusions can be drawn as follows.

1. The fracture energy indicators, *FI*, and *TI*, fail to significantly distinguish the effect of CR contents on the crack resistance of DREAM. In contrast, the *CRI*, *CRI*^{pre}, *TSI*, and *TS* indicators, which are normalized with respect to G_f or P_{max}, show satisfactory sensitivity to different DREAMs across varying test temperatures and loading rates. None of the nine fracture indicators can significantly distinguish the effects of loading rate for all DREAMs, as the brittleness of DREAM increases the variability in fracture energy indicators among replicates at the three loading rates. The *TSI, CRI*, and *CRI*^{pre} indicators meet the required adaptability only for DREAMs with high CR contents. Regarding the effect of test temperature, only the *TS*, *TSI*, and *CRI* parameters can significantly distinguish differences of DREAMs under the two test temperatures.

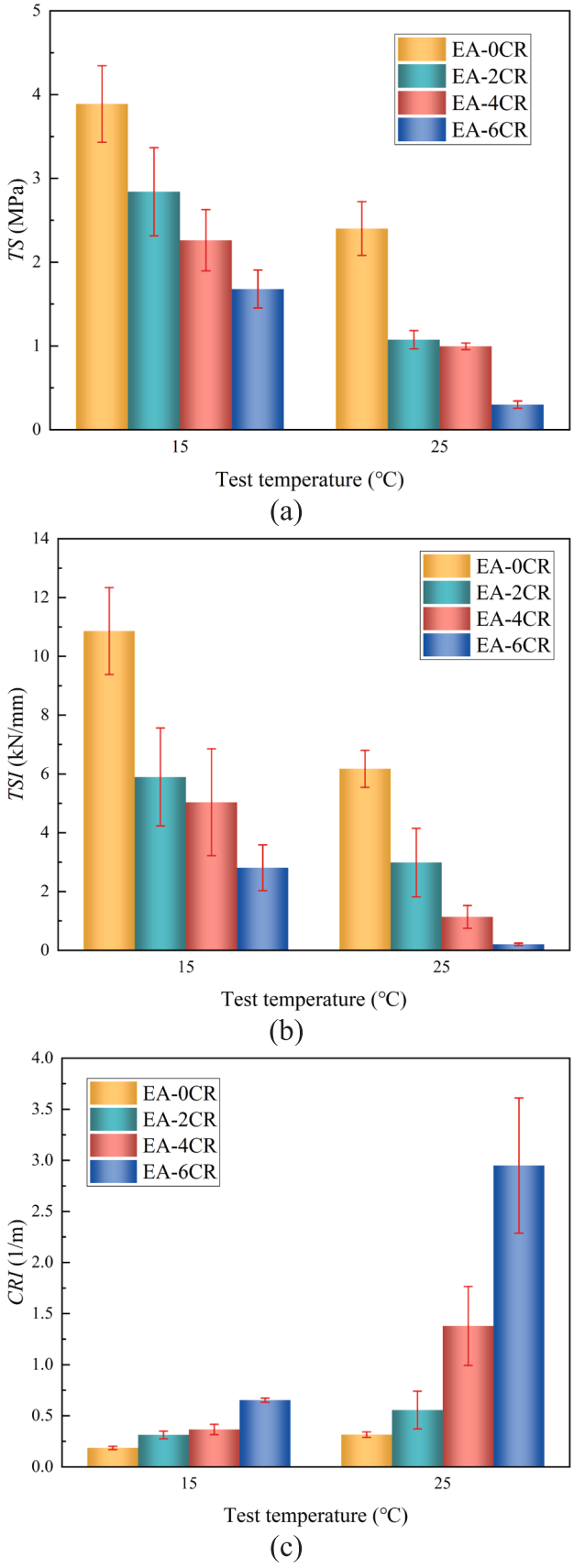

Fig. 7. Fracture indicators of DREAM at a loading rate of 1 mm/min and two test temperatures: (a) TS; (b) TSI; (c) CRI.

Table 10
Relative changes in three parameters of each DREAM when decreasing the test temperature from 25 to 15 °C.

Relative change in (%)	TS	TSI	CRI
EA-0CR	61.9	75.8	−41.2
EA-2CR	164.4	97.6	−43.8
EA-4CR	127.2	342.7	−73.5
EA-6CR	459.5	1262.3	−77.9

2. The *CRI*, CRI_{pre}, *TSI*, and *TS* indicators suggest that the addition of CR decreases the peak load-bearing capacity and stiffness of DREAM, while enhancing its flexibility. The DREAMs become less brittle, thereby improving their performance in crack propagation resistance after crack formation. A balanced evaluation is suggested to be conducted when applying DREAM in engineering, as a higher CR content is preferred to improve crack propagation resistance, provided that the fracture strength requirements are satisfied.
3. The variation trend of *TSI* with loading rate differs between DREAMs with low and high CR content. This suggests that CR decreases the stiffness of DREAM at higher loading rates while simultaneously reducing its capacity to withstand peak loads. The *TSI* shows greater sensitivity to changes in loading rate compared to CRI^{pre} and *CRI*. At higher loading rates, the improvement in DREAM toughness due to CR becomes more pronounced.
4. Analysis of fracture indicators indicates that reducing the test temperature to 15 °C results in increased values of both *TS* and *TSI* for each DREAM, whereas *CRI* decreases. Similar to the results of increasing the loading rate, *TS*, *TSI*, and *CRI* parameters become more sensitive to the test temperature as the CR content rises. Additionally, *TS* and *TSI* are more sensitive to test temperature compared to *CRI*.

This study is based on macroscopic mechanical experiments aimed at calculating various fracture parameters of different DREAMs and analyzing their sensitivity to CR content and loading conditions. Future research will employ microscopic experiments and multi-scale approaches to elucidate the mechanisms behind the influence of CR, loading rate, and temperature on DREAM.

CRediT authorship contribution statement

Chenguang Shi: Writing – review & editing, Methodology, Investigation, Formal analysis, Conceptualization. **Tianling Wang:** Writing – review & editing, Writing – original draft, Visualization, Methodology, Formal analysis. **Peng Guo:** Methodology, Formal analysis. **Yulou Fan:** Formal analysis, Data curation. **You Wu:** Methodology, Conceptualization. **Jun Yang:** Writing – review & editing, Supervision, Resources, Funding acquisition.

Declaration of competing interest

The authors declare that they have no known competing financial interests or personal relationships that could have appeared to influence the work reported in this paper.

Acknowledgments

The authors acknowledge the financial support of the National Natural Science Foundation of China (No. 52078130, No. 52378444), Chongqing Talents Program Project (CSTC2024YCJH-BGZXM0104), Chongqing Technology Innovation and Application Development Special Key Project (CSTB2022TIAD-KPX0203), Major Projects of the Science and Technology Research Plan of Chongqing Municipal Education Commission (KJZD-M202400704), Chongqing Talent Innovation Demonstration Team (CQYC202203091112), and Joint Training Base

Construction Project for Graduate Students in Chongqing (JDLHPYJD2020013, JDLHPYJD2021010).

Data availability

Data will be made available on request.

References

[1] C. Shi, et al., Design and performance evaluation of Bi-block precast rubberized epoxy asphalt trackbed for railway, Constr. Build. Mater. 313 (2021).
[2] F. Soto, G. Mino, Improvements in the mix-design, performance features and rational methodology of rubber modified binders for the thermal evaluation of the railway sub-ballast, Int. J. Res. Sci. Manage. 5 (2) (2018) 1–22.
[3] F. Soto, G. Mino, Volumetric Mix-Design optimization of bituminous rubber-mixtures in railway sub-ballast, Int. J. Eng. Sci. Res. Technol. 7 (1) (2018) 483–507.
[4] Soto, F.M., Characterization of rubberized asphalt for railway sub-ballast. Improvements in the mix-design, performance features and rational methodology of HMA_RUMAC blends for railways. 2018: Lambert Academic Publishing.
[5] T. Wang, et al., Mechanical properties evaluation of crumb rubber asphalt mixture for elastic trackbed, Constr. Build. Mater. 331 (2022).
[6] C. Shi, et al., Analysis of crumb rubber content influence on damage evolution and pattern recognition of rubberised epoxy asphalt mixture using acoustic emission techniques, Int. J. Pavement Eng. 25 (1) (2024).
[7] P. Men, et al., On use of polyvinylpyrrolidone to modify polyethylene fibers for improving tensile properties of high strength ECC, Constr. Build. Mater. 417 (2024).
[8] F. Safazadeh, et al., Methods to evaluate intermediate temperature properties of asphalt mixtures by the semi-circular bending (SCB) test, Road Mater. Pavement Des. (2021).
[9] F. Safazadeh, et al., Practicality of driven parameters of semicircular bending test at intermediate temperature, J. Transp. Eng. Part B-Pavements 147 (3) (2021).
[10] H. Alkuime, et al., Development of a new performance indicator to evaluate resistance of asphalt mixes to cracking, J. Transp. Eng. Part B-Pavements 146 (4) (2020).
[11] D.X. Lu, M. Saleh, N.H.T. Nguyen, Evaluation of fracture and fatigue cracking characterization ability of nonstandardized semicircular-bending test for asphalt concrete, J. Mater. Civ. Eng. 32 (8) (2020).
[12] Q. Guo, et al., Influence of wet-dry history on the mixed fracture properties of dense asphalt mixture based on ASCB test, Theor. Appl. Fract. Mech. 137 (2025).
[13] Q. Guo, et al., Investigation of the low-temperature properties and cracking resistance of fiber-reinforced asphalt concrete using the DIC technique, Eng. Fract. Mech. 229 (2020).
[14] Q. Guo, et al., Laboratory evaluation on performance of diatomite and glass fiber compound modified asphalt mixture, Mater. Des. 66 (2015) 51–59.
[15] Q. Guo, et al., Effect of wet-dry history on performances of dense asphalt mixture: Experimental investigation and predicting model, Constr. Build. Mater. 426 (2024).
[16] Q. Guo, et al., Influence of basalt fiber on mode I and II fracture properties of asphalt mixture at medium and low temperatures, Theor. Appl. Fract. Mech. 112 (2021).
[17] J. Zhang, et al., Characterization of crack growth rate of sulfur-extended asphalt mixtures using cyclic semicircular bending test, J. Mater. Civ. Eng. 30 (12) (2018).
[18] V. Venudharan, K.P. Biligiri, Investigation of cracking performance of asphalt-rubber gap-graded mixtures: Statistical overview on materials' interface, J. Test. Eval. 47 (5) (2019) 3336–3354.
[19] A.A. Soliman, R.N. Laoulache, W.S. Mogawer, Crack propagation characterization of asphalt mixtures: Weibull distribution and entropy approach, J. Mater. Civ. Eng. 32 (3) (2020).
[20] G. Saha, K.P. Biligiri, Modulus prediction of asphalt mixtures using dynamic semicircular bending test: Estimation algorithm and nomograph development, Int. J. Fatigue 109 (2018) 137–144.
[21] L. Espinosa, S. Caro, J. Wills, Study of the influence of the loading rate on the fracture behaviour of asphalt mixtures and asphalt mortars, Constr. Build. Mater. 262 (2020).
[22] Q. Li, X. Li, T. Yin, Effect of microwave heating on fracture behavior of granite: An experimental investigation, Eng. Fract. Mech. 250 (2021).
[23] A. Mahmoudi, et al., On the evaluation of entropy threshold for debonding during crack prorogation using DIC technique, Eng. Fract. Mech. 288 (2023).
[24] T. Meng, et al., Study of mode II fracture characteristics and roughness in salt rock after treatment coupled thermo-hydro-mechanical environment, Eng. Fract. Mech. 291 (2023).
[25] F. Xue, Z. Lin, T. Wang, Experimental study on effects of cyclic loading paths on cracking behavior and fracture characteristics of granite, Eng. Fract. Mech. 295 (2024).
[26] Al-Qadi, I.L., et al., Testing Protocols to Ensure Performance of High Asphalt Binder Replacement Mixes Using RAP and RAS, in A report of the findings of ICT-R27-128. Illinois Center for Transportation Series No. 15-017. Research Report No. FHWA-ICT-15-017. 2015, Illinois Center for Transportation.
[27] F. Pérez-Jiménez, et al., Analysis of the mechanical behaviour of bituminous mixtures at low temperatures, Constr. Build. Mater. 46 (2013) 193–202.
[28] F. Kaseer, et al., Development of an index to evaluate the cracking potential of asphalt mixtures using the semi-circular bending test, Constr. Build. Mater. 167 (2018) 286–298.
[29] H. Ozer, et al., Development of the fracture-based flexibility index for asphalt concrete cracking potential using modified semi-circle bending test parameters, Constr. Build. Mater. 115 (2016) 390–401.
[30] S. Im, Y.-R. Kim, H. Ban, Rate- and temperature-dependent fracture characteristics of asphaltic paving mixtures, J. Test. Eval. 41 (2) (2013) 257–268.
[31] M. Zarei, et al., Evaluation of fracture behaviour of modified warm mix asphalt containing vertical and angular cracks under freeze-thaw damage, Int. J. Pavement Eng. 24 (2) (2022).
[32] S. Pirmohammad, M. Abdi, M.R. Ayatollahi, Effect of support type on the fracture toughness and energy of asphalt concrete at different temperature conditions, Eng. Fract. Mech. 254 (2021).
[33] X. Chen, M. Solaimanian, Effect of test temperature and displacement rate on semicircular bend test, J. Mater. Civ. Eng. 31 (7) (2019).
[34] F. Zhou, et al., Selection and preliminary evaluation of laboratory cracking tests for routine asphalt mix designs, Road Mater. Pavement Des. 18 (2017) 62–86.
[35] J. Li, et al., Laboratory improvement and field assessment of Volumetric design method based on multi-point Supported skeleton for asphalt mixtures (V-S method), Constr. Build. Mater. 224 (2019) 962–979.
[36] J. Li, et al., Two-step improvements of volumetric design method based on multi-point supported skeleton for asphalt mixtures, Constr. Build. Mater. 217 (2019) 456–472.
[37] M. Fakhri, E.H. Kharrazi, M.R.M. Aliha, Mixed mode tensile – In plane shear fracture energy determination for hot mix asphalt mixtures under intermediate temperature conditions, Eng. Fract. Mech. 192 (2018) 98–113.
[38] H.R. Hajiloo, et al., Crack resistance of fiber-reinforced asphalt mixtures: Effect of test specimen and test condition, Fatigue Fract. Eng. Mater. Struct. 45 (3) (2022) 921–937.
[39] X. Li, M. Marasteanu, The fracture process zone in asphalt mixture at low temperature, Eng. Fract. Mech. 77 (7) (2010) 1175–1190.
[40] Y. Zhu, et al., Comprehensive evaluation of low-temperature fracture indices for asphalt mixtures, Road Mater. Pavement Des. 18 (sup4) (2017) 467–490.